

**EXPERIMENTAL AND NUMERICAL STUDIES ON THERMAL ANALYSIS  
OF HEAT PIPES FOR COMPUTER COOLING APPLICATIONS**

**by**

**MOHAMED H A ELNAGGAR**

**Thesis submitted in fulfillment of the  
requirements for the degree of  
Doctor of Philosophy**

**July 2012**

## **DEDICATION**

This thesis is dedicated to my beloved parents for their prayers and tremendous sacrifices. They are always a constant source of inspiration and motivation in my life. Their support and love have pulled me throughout my difficult times. Not to forget my lovely wife, daughters and sons.

Mohamed H A Elnaggar

July 2012

## ACKNOWLEDGEMENTS

بسم الله الرحمن الرحيم والصلاة والسلام على سيدنا محمد أشرف الأنبياء والمرسلين

First and foremost, I wish to thank Allah who gave me the opportunity to accomplish my studies.

I would like to express my highest gratitude and appreciation to my supervisor, Prof. Dr. Mohamad Zulkifly Abdullah, for his guidance, advice and endless encouragement throughout this research. My sincere appreciation is also extended to Prof. M. Abdul Mujeebu who has been a source of inspiration and guidance throughout this research. I sincerely would like to thank all the academic staff, technicians and colleagues in the School of Mechanical Engineering (USM) for their courtesy, help, and support.

I wish to acknowledge Universiti Sains Malaysia (USM) for the financial support extended under the USM fellowship scheme. This support enabled me concentrate on my research; I will always feel indebted to USM as well as the peaceful country of Malaysia. My deepest gratitude is indeed extended to the Palestinian Ministry of Education and Higher Education, and Palestine Technical College, for providing me with this opportunity to pursue my PhD.

My special thanks are due to my friends Mr. Sufian, Dr. Khalil, Mr. Zubair, Mr. Nazmi, Mr. Motasem and Dr. Hussam Abu Shawish, without whose help, this research would not have been successful. Last but not the least, I express my gratitude to my family members and all those who helped me in the smooth completion of this work.

## TABLE OF CONTENTS

DEDICATION	ii
ACKNOWLEDGEMENTS	iii
TABLE OF CONTENTS	iv
LIST OF TABLES	x
LIST OF FIGURES	xii
LIST OF SYMBOLS	xxiii
LIST OF ABBREVIATION	xxvii
LIST OF PUBLICATIONS	xxviii
ABSTRAK	xxix
ABSTRACT	xxx
<b>CHAPTER 1: INTRODUCTION</b>	
1.1 Introduction	1
1.2 Heat Pipe	1
1.2.1 Historical background	3
1.2.2 Construction of heat pipe	3
1.2.3 Heat pipe theory and operation	8
1.2.4 Effective thermal resistance of heat pipe	9
1.2.5 Advantages of heat pipe	9
1.3 Heat pipe for electronic cooling	10
1.4 Problem Statement	11

1.5 Research Objectives	14
1.6 Thesis Outline	14
<b>CHAPTER 2: LITERATURE REVIEW</b>	
2.1 Cooling methods of electronic equipments	16
2.2 Thermal Design Power (TDP)	17
2.3 Experimental studies of the heat pipe	18
2.4 Types of heat pipes	21
2.4.1 Cylindrical heat pipe	21
2.4.2 Flat heat pipes	23
2.4.3 Micro heat pipes	24
2.4.4 Heat pipe with Fins	28
2.5 Mathematical model	31
2.5.1 Analytical method	31
2.5.2 Numerical modeling	33
2.5.2.1 Two dimensional modeling	34
2.5.2.2 Three dimensional modeling	37
2.6 Heat pipes components	40
2.6.1 Wick structure	40
2.6.2 Working fluids	45
2.6.3 Vapor flow	47
2.7 Heat pipe for electronic cooling (Desktop and notebook)	49
2.8 Concluding remarks	53

## **CHAPTER 3: MATERIALS AND METHODS**

3.1 Experimental procedure and analysis	55
3.1.1 U-shape vertical multi heat pipe	55
3.1.2 U-shape vertical twin heat pipe	62
3.1.3 L-shape horizontal flat heat pipe	69
3.2 Design of Experiment (DOE)	72
3.3 Error Analysis	74
3.3.1 Types of experimental errors	74
3.3.2 Mean, standard deviation and standard error	75
3.4 Numerical Simulation	76
3.4.1 Fundamental steps of FEM	77
3.4.2 Three dimensional heat conduction model for heat pipe	77
3.4.3 Thermal solid elements	78
3.4.4 Mesh generation	79
3.4.5 Governing equations	82
3.4.6 Boundary conditions	83
3.4.7 ANSYS/FLOTRAN	84
3.4.8 Main steps in ANSYS FLOTRAN	84
3.4.9 Two dimensional simulation of characterization of working fluid	85
3.4.9.1 ANSYS FLOTRAN Elements	85
3.4.9.2 U-shape heat pipe	86
3.4.9.3 L-shape heat pipe for notebook PC	92

3.4.9.4 Selection of FLOTTRAN CFD solver	94
3.4.9.5 Grid independence test	95
3.4.9.6 Analytical method	97

## **CHAPTER 4: RESULTS AND DISCUSSION**

### **Part - I**

4.1 Finned vertical U-shape multi heat pipe	99
4.1.1 Thermal analysis	99
4.1.2 Transient temperature distribution	107
4.1.3 Optimization Using DOE	108
4.1.3.1 Analysis of variance (ANOVA)	109
4.1.3.2 Interaction between variables, and optimization	112
4.1.4 3D Simulations results	114
4.1.5 Comparison of experimental and simulation results	118

### **Part – II**

4.2 U-Shape twin heat pipe	118
4.2.1 Thermal analysis	118
4.2.2 Transient temperature distribution of the twin U-shape heat pipe	125
4.2.3 Optimization Using DOE	126
4.2.4 3D Simulation results	131
4.2.4.1 Natural convection	131

4.2.4.2 Forced Convection	134
4.2.4.3 Comparison of experimental and simulation results	136
4.2.5 2D simulation Results of characterization of working fluid	137
4.2.5.1 Wall temperature	137
4.2.5.2 Vapor velocity	141
4.2.5.3 Vapor and liquid pressures	143
4.2.5.4 Effect of using methanol as working fluid	147
4.2.5.4 Effect of using Screen mesh wick	148

### **Part – III**

4.3 Horizontal finned L-shape flat heat pipe for notebook	154
4.3.1 Thermal resistance analysis	154
4.3.2 Transient temperature distribution of horizontal flat heat pipe	159
4.3.3 Effective thermal conductivity	162
4.3.4 Optimization Using DOE	163
4.3.5 3D simulation results	168
4.3.5.1 Natural convection	168
4.3.5.2 Forced convection	170
4.3.6 2D simulation results of characterization of working fluid	172
4.3.6.1 Wall temperature	172
4.3.6.2 Comparison of experimental with simulation results	176
4.3.6.3 Vapor velocity	177
4.3.6.4 Liquid velocity	178



4.3.6.5 Vapor and liquid pressures	180
4.3.6.6 Effect of increasing the wick thickness	186
4.3.6.7 Effect of using screen mesh wick	190
4.3.7 Optimization results using D-optimal	221
4.3.7.1 Factors definition	221
4.3.7.2 Interaction between Factors and optimization	223
4.3.8 Results of analytical study	226
4.3.8.1 Natural convection	226
4.3.8.2 Forced convection	227
4.3.8.3 Comparison of analytical and simulation results	227
4.4 Results of error analysis	228
<b>CHAPTER 5: CONCLUSION AND FUTURE SCOPE</b>	
5.1 Concluding remarks	230
5.2 Recommendation for future work	234
<b>REFERENCES</b>	236

## LIST OF TABLES

		<b>Page</b>
Table 1.1	Heat pipe working fluids properties	5
Table 2.1	Maximum TDP for modern desktop computers	17
Table 2.2	Maximum TDP for modern notebook computers	18
Table 2.3	An overview of the main mathematical studies on heat pipes	38
Table 3.1	Finned U-shape multi heat pipe specifications	57
Table 3.2	Twin U-shaped heat pipe specifications	64
Table 3.3	Specifications finned flat heat pipe for notebook	70
Table 3.4	The default values used in ANSYS-FOLTRAN	91
Table 4.1	Independent variables of the CCD design	108
Table 4.2	Response values for different experimental conditions	109
Table 4.3	ANOVA for analysis of variance and adequacy of the quadratic model	110
Table 4.4	The optimization solutions of heat input and coolant velocity	114
Table 4.5	Material properties of U-shape multi heat pipe	115
Table 4.6	Comparison of experimental and simulation temperatures	118
Table 4.7	Independent variables of the CCD design	127
Table 4.8	Response values for different experimental conditions	127
Table 4.9	ANOVA for analysis of variance and adequacy of the quadratic model	128
Table 4.10	The optimization solutions of heat input and coolant velocity	131
Table 4.11	Material properties of U-Shape twin pipe	132
Table 4.12	Comparison of experimental and simulation temperatures	137

Table 4.13	The physical properties of water and vapor at 98°C	137
Table 4.14	Comparison of experimental and predicted temperatures	141
Table 4.15	Independent variables of the CCD design	164
Table 4.16	Response values for different experimental conditions	164
Table 4.17	ANOVA for analysis of variance and adequacy of the quadratic model	164
Table 4.18	The optimization solutions of heat input and coolant airflow rate	168
Table 4.19	The physical properties of water and vapor at 120 °C	173
Table 4.20	Comparison of experimental with 3D and 2D simulation temperatures	177
Table 4.21	The physical properties of liquid and vapor of methanol at 120 °C	197
Table 4.22	Factors of D-Optimal design	221
Table 4.23	Response values for different simulation conditions	222
Table 4.24	Comparison of analytical and numerical results at natural convection	227
Table 4.25	Comparison of analytical and numerical results at forced convection	228
Table 4.26	Error analysis for temperature measurements of finned U-shape multi heat pipe	228
Table 4.27	Error analysis for temperature measurements of finned U-shape twin heat pipe	229
Table 4.28	Error analysis for temperature measurements of finned flat L-shape twin heat pipe	229

## LIST OF FIGURES

		<b>Page</b>
Figure 1.1	Heat pipe operation	2
Figure 1.2	Metal sintered Powder wick	6
Figure 1.3	Grooved wick	6
Figure 1.4	Screen Mesh wick	7
Figure 2.1	Experimental setups (a) Steady-state test (b) Dynamic test	20
Figure 2.2	Coordinate system of the heat pipe	22
Figure 2.3	Schematic of the flat plate heat pipe	23
Figure 2.4	Geometry of different cross-sectional shape of micro-heat pipes	28
Figure 2.5	Schematic of inner fin's structure	30
Figure 2.6	Comparison of the calculated vapor and liquid pressure distributions	32
Figure 2.7	Predict the velocity distribution of the vapor along the heat pipe	35
Figure 2.8	Heat pipe model and coordinate system	36
Figure 2.9	Heat pipe heat sink solution for cooling desktop PCs	49
Figure 2.10	The temperature difference vs. the heat input	50
Figure 2.11	Heat sink without and with embedded heat pipes	52
Figure 2.12	Total thermal resistance at various heat inputs	53
Figure 3.1	Finned U shape multi-heat pipe	56
Figure 3.2	Details of the finned heat pipe	56
Figure 3.3	Experimental apparatus for U-shape multi heat pipe	58
Figure 3.4	Dimensions and thermocouple locations of U-shape multi heat pipe	59

Figure 3.5	Thermal resistance network for U-shape multi heat pipe	61
Figure 3.6	The finned U-shape twin heat pipe with explicit details	63
Figure 3.7	Thermocouple locations for U-shape twin heat pipe	65
Figure 3.8	Thermal resistance network of U-shape twin heat pipes	68
Figure 3.9	Cross-section of flat heat pipe and equivalent diameter	69
Figure 3.10	Finned L-shape flat heat pipe for notebook PC cooling	70
Figure 3.11	Experimental apparatus for finned L-shape flat heat pipe	71
Figure 3.12	Thermal resistance network of finned L-shape flat heat pipe	72
Figure 3.13	SOLID70 Element used by ANSYS	79
Figure 3.14	The meshed simulation model finned U-shape multi heat pipe	80
Figure 3.15	The meshed simulation model of finned twin U-shaped heat pipe	81
Figure 3.16	The meshed simulation model of finned L-shape flat heat pipe	82
Figure 3.17	FLUID141 for two dimensional Fluid-Thermal Element	85
Figure 3.18	The meshed simulation model of vapor domain	93
Figure 3.29	The meshed of liquid-wick structure and the heat pipe wall domains	93
Figure 3.20	Checking for mesh accuracy for U-shape multi heat pipe	95
Figure 3.21	Checking for mesh accuracy for U-shape twin heat pipe	96
Figure 3.22	Checking for mesh accuracy for L-shape heat pipe	97
Figure 4.1	Thermal resistances of half U-shape heat pipe ( $R_h$ ) versus heat input at various coolant velocities, and in natural convection	100
Figure 4.2	Thermal resistances of the full single U-shape heat pipe ( $R_{hp}$ ) versus heat input at various coolant velocities, and in natural convection	101
Figure 4.3	Thermal resistances of the base plate ( $R_b$ ) versus heat input at various coolant velocities, and in natural convection	102

Figure 4.4	Thermal resistances of heat pipe-fin convective ( $R_f$ ) versus heat input at various coolant velocities, and in natural convection	103
Figure 4.5	Temperature difference between condenser sections and ambient ( $T_c - T_a$ ) versus heat input at various coolant velocities, and in natural convection	104
Figure 4.6	Thermal resistance versus heat input in natural convection	105
Figure 4.7	Total thermal resistance versus heat input	106
Figure 4.8	Heat transfer coefficient vs. Reynolds number	107
Figure 4.9	Transient temperature distribution within the finned U-shape heat pipe	109
Figure 4.10	Normal probability plot of studentized residuals	111
Figure 4.11	Predicted versus actual values of $R_t$	112
Figure 4.12	2D contour plots of $R_t$ as functions of $Q$ (A) and $V$ (B)	113
Figure 4.13	3D surface plots of $R_t$ as function of heat input (A) and coolant velocity (B)	114
Figure 4.14	Predicted temperature distribution in natural convection	115
Figure 4.15	Predicted temperature distribution in forced convection	116
Figure 4.16	Predicted transient temperature distribution at natural convection	117
Figure 4.17	Predicted transient temperature distribution in forced convection	117
Figure 4.18	Thermal resistances of the base plate ( $R_b$ ) versus $Q$ at various $V$ , and in natural convection	119
Figure 4.19	Thermal resistance of half U-shape heat pipe ( $R_{hp}$ ) versus $Q$ for natural and forced convection modes	120
Figure 4.20	Thermal resistance of full single U-shape heat pipe versus heat input for natural and forced convection modes	121
Figure 4.21	Thermal resistances of heat pipe-fin convective ( $R_f$ ) versus heat input in natural and forced convection modes	122

Figure 4.22	Total thermal resistance versus heat input at forced convection	123
Figure 4.23	Total thermal resistance versus heat input at natural convection	124
Figure 4.24	Temperature difference between condenser sections and ambient with varies heat input	125
Figure 4.25	Transient temperature distribution within the finned U-shape heat pipe	126
Figure 4.26	Normal probability plot of studentized residuals	128
Figure 4.27	Predicted versus actual values of $R_t$	129
Figure 4.28	Perturbation plot between heat input (A) and coolant air velocity (B)	130
Figure 4.29	3D surface plots of $R_t$ as function of heat input (A) and coolant velocity (B)	130
Figure 4.30	Predicted temperature distributions in Natural convection	132
Figure 4.31	Predicted temperature distribution of the base in natural convection	133
Figure 4.32	Predicted transient temperature distribution at natural convection	135
Figure 4.33	Predicted temperature distribution in forced convection	135
Figure 4.34	Predicted temperature distribution of the base in forced convection	135
Figure 4.35	Predicted transient temperature distribution at forced convection	136
Figure 4.36	Wall temperature distribution at natural convection U-shape heat pipe (Sintered-water)	138
Figure 4.37	Wall temperature distribution of U-shape heat pipe at forced convection ( $V=3$ m/s) (Sintered-water)	139
Figure 4.38	Predicted liquid (water) and wall temperature distributions of U-shape heat pipe in forced convection ( $V=3$ m/s) (Sintered-water)	140
Figure 4.39	The vapor velocity distribution within the heat pipe	142

Figure 4.40	Radial velocity distribution of condenser section at different y positions	142
Figure 4.41	Radial velocity distribution of evaporator section at different x positions	143
Figure 4.42	Vapor pressure distribution within the heat pipe	144
Figure 4.43	Liquid pressure distribution for different parts of the heat pipe	144
Figure 4.44	Liquid pressure distribution along the half of length of heat pipe	145
Figure 4.45	Vapor and Liquid pressure distribution of U-shape heat pipe	146
Figure 4.46	Liquid velocity along y direction	146
Figure 4.47	Wall temperature distribution of U-shape heat pipe in forced convection ( $V=3$ m/s) (Sintered-Methanol)	147
Figure 4.48	Liquid (Methanol) pressure distribution along heat pipe at $Q=10$ W at $V=3$ m/s (wick Sintered copper powder $K=1.17 \times 10^{-11}$ )	148
Figure 4.49	Wall temperature distribution of U-shape heat pipe in forced convection ( $V=3$ m/s) (Screen-water)	149
Figure 4.50	Wall temperature distribution of U-shape heat pipe in forced convection ( $V=3$ m/s) (Screen-Methanol)	150
Figure 4.51	Wall temperature distribution of U-shape heat pipe in forced convection ( $V=3$ m/s) with reference to variation of wick structure and working fluid	151
Figure 4.52	Liquid (Water) pressure distribution along heat pipe at $Q=10$ W at $V=3$ m/s (wick Screen mesh $K=1.93 \times 10^{-10}$ )	152
Figure 4.53	Liquid (Methanol) pressure distribution along U-shape heat pipe at $Q=10$ W at $V=3$ m/s (wick Screen mesh $K=1.93 \times 10^{-10}$ )	153
Figure 4.54	Liquid pressure distribution of U-shape heat pipe ( $Q_h=10$ W) in forced convection ( $V=3$ m/s) with various wick structures and working fluids	154
Figure 4.55	Total thermal resistance vs. heat input at natural convection	155
Figure 4.56	Total thermal resistance vs. heat input at varies coolant flow rate	156



Figure 4.57	Heat pipe thermal resistance vs. heat input at natural convection	157
Figure 4.58	Heat pipe thermal resistance vs. heat input at various coolant velocities	158
Figure 4.59	Thermal resistance of the base plate to heat pipe vs. heat input at various coolant airflow rates	158
Figure 4.60	Thermal resistance of heat pipe to fins vs. heat input at various coolant airflow rates	159
Figure 4.61	Transient temperature distribution with the finned flat heat pipe at $Q=20W$ at natural convection	160
Figure 4.62	Transient temperature distribution with the finned flat heat pipe at $Q=35 W$ and coolant airflow rate $5.5m^3/h$	161
Figure 4.63	Transient temperature distribution with the finned flat heat pipe at $Q=35W$ and coolant air flow rate, $6.5m^3/h$	162
Figure 4.64	Effective thermal conductivity of heat pipe vs. heat input at various coolant airflow rates	163
Figure 4.65	Normal probability plot of studentized residuals	166
Figure 4.66	Predicted versus actual values of $K_{eff}$ (W/mK)	166
Figure 4.67	Perturbation plot of heat input (A) and coolant airflow rate (B)	167
Figure 4.68	3D surface plots of $K_{eff}$ as function of heat input (A) and coolant airflow rate (B)	167
Figure 4.69	Temperature contour of finned flat heat pipe at $Q=20W$ in natural convection	169
Figure 4.70	Predicted transient temperature distribution with the finned heat pipe at $Q=20W$ at natural convection	170
Figure 4.71	Predicted temperature distribution at $Q=35 W$ and $Q^* = 6.5 m^3/h$	171
Figure 4.72	Predicted transient temperature distribution with the finned heat pipe at $Q=35W$ and $Q^*=6.5 m^3/h$	172
Figure 4.73	Predict temperature distribution at $Q=20 W$ and Natural Convection	174

Figure 4.74	Wall temperature distribution along the heat pipe at $Q=20$ W in natural convection	174
Figure 4.75	Predicted wall and liquid-wick region temperature distributions at $Q=35$ W with coolant airflow rate of $6.5$ m <sup>3</sup> /h.	175
Figure 4.76	Predicted temperature distribution along heat pipe at $Q=35$ W with coolant airflow rate of $6.5$ m <sup>3</sup> /h	176
Figure 4.77	Predict vapor velocity distribution at $Q=20$ W and natural convection	177
Figure 4.78	Predicted vapor velocity distribution along the heat pipe at $Q=35$ W with forced convection (coolant airflow rate $6.5$ m <sup>3</sup> /h)	178
Figure 4.79	Predicted liquid velocity distribution at $Q=20$ W under natural convection	179
Figure 4.80	Liquid vector velocity at $Q=20$ W in natural convection	179
Figure 4.81	Liquid velocity direction and distribution for different parts of the heat pipe at $Q=35$ W with forced convection (coolant airflow rate $6.5$ m <sup>3</sup> /h)	180
Figure 4.82	Predicted vapor pressure distribution at $Q=20$ W with natural convection	181
Figure 4.83	Predicted vapor pressure distribution at $Q=35$ W with forced convection	182
Figure 4.84	Liquid pressure distribution along heat pipe at $Q=20$ W with natural convection	183
Figure 4.85	Liquid pressure distribution along heat pipe at $Q=20$ W with natural convection	184
Figure 4.86	Vapor and liquid pressure distributions of the flat heat pipe at $Q=20$	184
Figure 4.87	Liquid pressure distribution along heat pipe at $Q=35$ W with coolant airflow rate of $6.5$ m <sup>3</sup> /h	185
Figure 4.88	Liquid pressure distribution along heat pipe at $Q=35$ W with coolant airflow rate of $6.5$ m <sup>3</sup> /h	186

Figure 4.89	Predicted water-wick region and wall temperature distribution at $Q=35$ W in forced convection ( $Q^*=6.5$ m <sup>3</sup> /h) with 0.75 mm sintered copper powder wick thickness	187
Figure 4.90	Predicted wall temperature distribution at $Q=35$ W in forced convection ( $Q^*=6.5$ m <sup>3</sup> /h) with 0.75 sintered copper powder wick thickness	187
Figure 4.91	Predicted liquid (water) pressure distribution at $Q=35$ W in forced convection ( $Q^*=6.5$ m <sup>3</sup> /h) with 0.75 mm sintered copper powder wick thickness	188
Figure 4.92	Predicted liquid (Water) pressure distribution at $Q=35$ W in forced convection ( $Q^*=6.5$ m <sup>3</sup> /h) with 0.75 sintered copper powder wick thickness	189
Figure 4.93	Predict liquid (Water) pressure distribution at $Q=35$ W in forced convection ( $Q^*=6.5$ m <sup>3</sup> /h) of sintered copper powder wick with various thicknesses	190
Figure 4.94	Predict liquid-wick region and wall temperature distribution at $Q=20$ W in natural convection (Screen mesh $K=1.93 \times 10^{-10}$ )	191
Figure 4.95	Wall temperature distribution along the heat pipe at $Q=20$ W in natural convection (Screen mesh $K=1.93 \times 10^{-10}$ )	191
Figure 4.96	Liquid (water) pressure distribution at $Q=20$ W in natural convection (Screen mesh $K=1.93 \times 10^{-10}$ )	192
Figure 4.97	Liquid pressure distribution along the heat pipe at $Q=20$ W in natural convection (Screen mesh $K=1.93 \times 10^{-10}$ )	193
Figure 4.98	Liquid pressure distribution along the heat pipe at $Q=20$ W in natural convection (wick thickness=0.75 mm with Screen mesh $K=1.93 \times 10^{-10}$ )	194
Figure 4.99	Liquid pressure distribution of the heat pipe at $Q=20$ W in natural convection (wick thickness=0.75 mm with Screen mesh $K=1.93 \times 10^{-10}$ )	194
Figure 4.100	Liquid and wall temperature distribution along the heat pipe at $Q=20$ W in natural convection (wick thickness=0.75 mm with Screen mesh $K=1.93 \times 10^{-10}$ )	195

Figure 4.101	Wall temperature distribution along the heat pipe at Q=20 W in natural convection (wick thickness=0.75 mm with Screen mesh $K=1.93 \times 10^{-10}$ )	296
Figure 4.102	Wall temperature distribution along the heat pipe at Q=20 W in natural convection (wick thickness=0.5 mm with Screen mesh $K=1.93 \times 10^{-10}$ )	197
Figure 4.103	Methanol-wick region and wall temperature distributions along the heat pipe at Q=20 W in natural convection (wick thickness=0.5 mm with Screen mesh $K=1.93 \times 10^{-10}$ )	198
Figure 4.104	Wall temperature distribution along the heat pipe at Q=20 W in natural convection (wick thickness=0.75 mm with Screen mesh $K=1.93 \times 10^{-10}$ )	199
Figure 4.105	Methanol-wick region and wall temperature distribution along the heat pipe at Q=20 W in natural convection (wick thickness=0.75 mm with Screen mesh $K=1.93 \times 10^{-10}$ )	200
Figure 4.106	wall temperature distribution of heat pipe in natural convection with reference to variation of working fluid and thicknesses of screen mesh wick ( $K=1.93 \times 10^{-10} \text{ m}^2$ ) at Q=20 W	201
Figure 4.107	Liquid pressure distribution of the heat pipe at Q=20 W in natural convection (wick thickness=0.5 mm with Screen mesh)	202
Figure 4.108	Liquid (Methanol) pressure distribution of the heat pipe at Q=20 W in natural convection (wick thickness=0.5 mm with Screen mesh $K=1.93 \times 10^{-10}$ )	202
Figure 4.109	Liquid (Methanol) pressure distribution of the heat pipe at Q=20 W in natural convection (wick thickness=0.75 mm with Screen mesh $K=1.93 \times 10^{-10}$ )	203
Figure 4.110	Liquid (Methanol) pressure distribution of the heat pipe at Q=20 W in natural convection (wick thickness=0.75 mm with Screen mesh $K=1.93 \times 10^{-10}$ )	204
Figure 4.111	Liquid pressure distribution along the heat pipe at Q=20 W in natural convection with various wick thicknesses (Screen mesh $K=1.93 \times 10^{-10}$ )	205

Figure 4.112	Liquid (water) pressure distribution of the heat pipe at Q=35 W at Q*=6.5 m <sup>3</sup> /h (wick thickness=0.5 mm with Screen mesh K=1.93x10 <sup>-10</sup> )	206
Figure 4.113	Liquid (water) pressure distribution of the heat pipe at Q=35 W at Q*=6.5 m <sup>3</sup> /h (wick thickness=0.5 mm with Screen mesh K=1.93x10 <sup>-10</sup> )	207
Figure 4.114	Liquid (Water)-wick region and wall temperature distribution along the heat pipe at Q=35 W at Q*=6.5 m <sup>3</sup> /h (wick thickness=0.5 mm Screen mesh K=1.93x10 <sup>-10</sup> )	208
Figure 4.115	Wall temperature distribution along the heat pipe at Q=35 W at Q*=6.5 m <sup>3</sup> /h (wick thickness=0.5 mm with Screen mesh K=1.93x10 <sup>-10</sup> Water)	209
Figure 4.116	Liquid (water) pressure distribution of the heat pipe at Q=35 W at Q*=6.5 m <sup>3</sup> /h (wick thickness=0.75 mm with Screen mesh K=1.93x10 <sup>-10</sup> )	209
Figure 4.117	Liquid (water) pressure distribution of the heat pipe at Q=35 W at Q*=6.5 m <sup>3</sup> /h (wick thickness=0.75 mm with Screen mesh K=1.93x10 <sup>-10</sup> )	210
Figure4.118	Water-wick region and wall temperature distributions along the heat pipe at Q=35 W at Q*=6.5 m <sup>3</sup> /h (wick thickness=0.75 mm with Screen mesh K=1.93x10 <sup>-10</sup> )	211
Figure 4.119	Wall temperature distribution along the heat pipe at Q=35 W at Q*=6.5 m <sup>3</sup> /h (wick thickness=0.75 mm with Screen mesh K=1.93x10 <sup>-10</sup> Water)	211
Figure 4.120	Liquid (methanol) pressure distribution of the heat pipe at Q=35 W at Q*=6.5 m <sup>3</sup> /h (wick thickness=0.5 mm with Screen mesh K=1.93x10 <sup>-10</sup> )	212
Figure 4.121	Liquid (Methanol) pressure distribution along heat pipe at Q=35 W at Q*=6.5 m <sup>3</sup> /h (wick thickness=0.5 mm with Screen mesh K=1.93x10 <sup>-10</sup> )	213
Figure 4.122	Liquid (Methanol)-wick region and wall temperature distribution of the heat pipe at Q=35 W at Q*=6.5 m <sup>3</sup> /h (wick thickness=0.5 mm with Screen mesh K=1.93x10 <sup>-10</sup> )	214

Figure 4.123	Wall temperature distribution along heat pipe at $Q=35$ W at $Q^*=6.5\text{m}^3/\text{h}$ (wick thickness=0.5 mm with Screen mesh $K=1.93\times 10^{-10}$ Methanol)	215
Figure 4.124	Liquid (Methanol) pressure distribution of the heat pipe at $Q=35$ W at $Q^*=6.5$ $\text{m}^3/\text{h}$ (wick thickness=0.75 mm with Screen mesh $K=1.93\times 10^{-10}$ )	216
Figure 4.125	Liquid (Methanol) pressure distribution along heat pipe at $Q=35$ W at $Q^*=6.5$ $\text{m}^3/\text{h}$ (wick thickness=0.75 mm with Screen mesh $K=1.93\times 10^{-10}$ )	216
Figure 4.126	Methanol-wick region and wall temperature distributions of the heat pipe at $Q=35$ W at $Q^*=6.5$ $\text{m}^3/\text{h}$ (wick thickness=0.75 mm with Screen mesh $K=1.93\times 10^{-10}$ methanol)	217
Figure 4.127	Wall temperature distribution along heat pipe at $Q=35$ W at $Q^*=6.5\text{m}^3/\text{h}$ (wick thickness=0.75 mm with Screen mesh $K=1.93\times 10^{-10}$ Methanol)	218
Figure 4.128	Wall temperature distribution along the heat pipe at $Q=35\text{W}$ and forced convection ( $Q^*=6.5$ $\text{m}^3/\text{h}$ ) with various working fluid and wick types and thicknesses	219
Figure 4.129	Liquid pressure distribution along the heat pipe at $Q=35\text{W}$ at $Q^*=6.5$ $\text{m}^3/\text{h}$ with various working fluid and wick thickness at Screen mesh $K=1.93\times 10^{-10}$	220
Figure 4.130	3D surface for temperature difference ( $\Delta T$ ) and pressure drop ( $\Delta P_1$ ) as a function of wick thickness and wick permeability for the; (a) water- $\Delta T$ , (b) water- $\Delta P_1$ , (c) methanol- $\Delta T$ , (d) methanol- $\Delta P_1$	224

## LIST OF SYMBOLS

### English Symbols

$A_w$	Wick cross-sectional area $m^2$
$C$	The FLOTRAN permeability expressed in $m^{-2}$ , which is inverse of the physical permeability
$C_p$	Specific heat $J/kgK$
$f$	Friction coefficient
$g$	Acceleration of gravity $m^2/s$
$h_{fc}$	Heat transfer coefficient $W/m^2 K$
$h_{nc}$	Heat transfer coefficient at natural convection $W/m^2 K$
$K$	Wick permeability $m^2$
$k$	Number of independent variables
$k_{air}$	Thermal conductivity of air $W/mK$
$k_e$	Effective thermal conductivity of the liquid-wick structure $W/mK$
$K_{eff}$	Effective thermal conductivity of the heat pipe $W/mK$
$k_l$	Liquid thermal conductivity $W/mK$
$k_s$	Solid thermal conductivity $W/mK$

$k_v$	Vapor thermal conductivity	W/mK
$k_w$	Thermal conductivity of wick material	W/mK
$L_{ad}$	Adiabatic section length	m
$L_c$	Condenser section length	m
$L_e$	Evaporator section length	m
$L_{eff}$	Effective length of the heat pipe	m
$Nu$	Nusselt number	
$P_l$	Liquid pressure	(Pa)
$P_v$	Vapor pressure	(Pa)
$\Delta P$	Pressure drop	(Pa)
$Q$	Heat input	W
$Q_{hp}$	Heat input of single heat pipe	(W)
$q$	Heat flux	(W/m <sup>2</sup> )
$Q^*$	Coolant airflow rate	(m <sup>3</sup> /h)
$q^*$	Heat generate rate	(W/m <sup>3</sup> )
$R$	Thermal resistance	(°C/W)
$R_0$	Outside radius of the heat pipe	(m)



$R_b$	Base thermal resistance ( $^{\circ}\text{C}/\text{W}$ )
$R_{cb}$	The contact thermal resistance between heat source and the base plate ( $^{\circ}\text{C}/\text{W}$ )
$R_{ch}$	The contact thermal resistance between heat source and evaporator section ( $^{\circ}\text{C}/\text{W}$ )
$r_{\text{eff}}$	Effective pores radius of the wick (m)
$R_f$	Fins thermal resistance ( $^{\circ}\text{C}/\text{W}$ )
$R_h$	Thermal resistance of half U-shape heat pipe ( $^{\circ}\text{C}/\text{W}$ )
$R_{hp}$	Heat pipe thermal resistance ( $^{\circ}\text{C}/\text{W}$ )
$R_t$	Total thermal resistance ( $^{\circ}\text{C}/\text{W}$ )
$R_v$	Vapor core radius of heat pipe (m)
$R_w$	Wall inner radius of the heat pipe (m)
$R_x$	Distributed resistance in x direction $\text{N}/\text{m}^3$
$R_y$	Distributed resistance in y direction $\text{N}/\text{m}^3$
$s$	Distance between two fins (m)
$T$	Temperature $^{\circ}\text{C}$
$t$	Time (s)
$T_a$	Ambient temperature $^{\circ}\text{C}$
$T_{\text{ad}}$	Adiabatic section temperature $^{\circ}\text{C}$

$T_b$	Base plate temperature °C
$T_c$	Condenser temperature °C
$T_e$	Evaporator temperature °C
$T_{int}$	Interface temperature °C
$T_{sr}$	Source temperature °C
$T_s$	Heat pipe wall (surface) temperature °C
$u$	Velocity in x direction m/s
$u_1$	Vapor suction velocity m/s
$v$	Velocity in y directions m/s
$v$ and $u$ Subscripts refers to vapor and liquid regions respectively.	
$v_1$	Vapor injection velocity m/s
$x, y, z$	Space coordinates

### **Greek Symbols**

$\beta_0$	Constant coefficient
$\beta_j$	Interaction coefficient of linear
$\beta_{jj}$	Interaction coefficient of quadratic
$\beta_{ij}$	Interaction coefficient of the second-order terms

$\varepsilon$	Error
$\rho_l$	Liquid density $\text{kg/m}^3$
$\eta$	Normal vector
$\rho_v$	Vapor density $\text{kg/m}^3$
$\mu_v$	Vapor dynamic viscosity
$\mu_l$	Liquid dynamic viscosity $\text{Ns/m}^2$
$\phi$	Wick porosity
$\sigma_l$	Surface tension $\text{N/m}$

### **LIST OF ABBREVIATION**

CCD	Central Composite Design
CPU	Central Processing Unit of a computer microprocessor
DOE	Design of experiment
FEM	Finite Element Method
MHP	Miniature Heat Pipe
RSM	Response surface methodology

## LIST OF PUBLICATIONS

### International Journals

- ELNAGGAR, M. H. A., ABDULLAH, M. Z. & ABDUL MUJEEBU, M. 2011. Experimental analysis and FEM simulation of finned U-shape multi heat pipe for desktop PC cooling. Energy Conversion and Management, 52, 2937-2944. (ISI IF= 2.054)
- ELNAGGAR, M. H. A., ABDULLAH, M. Z. & MUJEEBU, M. A. 2011. Experimental Investigation and Optimization of Heat Input and Coolant Velocity of Finned Twin U-Shaped Heat Pipe for CPU Cooling. Experimental Techniques, (In press). (ISI IF= 0.5)
- ELNAGGAR, M. H. A., ABDULLAH, M. Z. & ABDUL MUJEEBU, M. 2012. Characterization of Working Fluid in Vertically Mounted Finned U-Shape Twin Heat Pipe for Electronic Cooling. Energy Conversion and Management, 62, 31-39. (ISI IF= 2.054)
- ELNAGGAR, M. H. A., ABDULLAH, M. Z. 2012. Experimental and Numerical Study of Finned L-shape Flat Heat Pipe for Notebook PC cooling. International Journal of heat and mass transfer, (Under review).
- ELNAGGAR, M. H. A., ABDULLAH, M. Z. 2012. Development of Heat Pipe and Application in Electronic Cooling-A comprehensive Survey. Applied Thermal Engineering, (Under review)

### Conference proceedings:

- ELNAGGAR, M. H. A., ABDULLAH, M. Z. 2010. Improving Forced Air Convection Heat transfer of Finned Heat Pipes. The First International Conference on Basic & Applied Sciences. Gaza, Palestine.
- ELNAGGAR, M. H. A., ABDULLAH, M. Z. 2011. Experimental Investigation And Optimization Of Coolant Flow Rate And Heat Input Of Finned Heat Pipe For Notebook Pc Cooling. 2nd Symposium of USM Fellowship Holders 2011, November 23-24, Vistana Hotel, Penang, Malaysia.
- ELNAGGAR, M. H. A., ABDULLAH, M. Z. 2011. Experimental and Numerical Investigation of Finned Multi Heat Pipe. 1st Mechanical & Aerospace Engineering Research Colloquium (MAERC 2010), Universiti Sains Malaysia 9 – 10 June 2010.

# **KAJIAN EKSPERIMEN DAN BERANGKA KE ATAS ANALISA TERMA BAGI PAIP HABA UNTUK APLIKASI PENYEJUKAN KOMPUTER**

## **ABSTRAK**

Dalam industri komputer, peningkatan pembangunan dan permintaan bagi kuasa pemprosesan memerlukan reka bentuk yang cekap untuk pemproses menjalankan operasi dengan pantas; justeru teknik penyejukan diperlukan bagi menyelerakkan haba yang terlibat adalah penting. Oleh itu, kajian amat diperlukan bagi menyelidik peranti penyejukan berpotensi tinggi terutamanya penyejukan CPU. Dalam kajian ini, paip haba berbentuk pelbagai dan berkembar-U, dan paip haba mengufuk berbentuk-L telah dikaji secara eksperimen dan berangka. Analisa terma dijalankan pada kedua-dua mod perolakan tabie dan paksa. Simulasi telah dijalankan dengan dua model; pertama model 3D berdasarkan pemindahan haba secara konduksi yang mana paip haba secara keseluruhannya dimodelkan dengan anggapan sebuah media berkonduksi, tanpa mengambil kira keadaan yang berlaku di dalam paip haba. Kedua adalah model 2D bagi mencirikan bendalir bekerja di dalam paip haba. Sebuah pengalatan terbaik bagi reka bentuk eksperimen (DOE) digunakan untuk mengoptimum halaju penyejuk dan haba masukan bagi menghasilkan prestasi terbaik bagi paip haba. Keputusan menunjukkan halaju udara dan kuasa masukan mempunyai kesan ketara ke atas prestasi paip haba yang bersirip. Jumlah rintangan terma menurun dengan peningkatan haba masukan dan halaju penyejuk. Nilai terendah bagi jumlah rintangan terma untuk paip haba pelbagai bentuk U bersirip, paip haba berkembar dan bentuk L tunggal masing-masing adalah  $0.181\text{ }^{\circ}\text{C/W}$ ,  $0.125^{\circ}\text{C/W}$  and  $0.533\text{ }^{\circ}\text{C/W}$ . Dalam simulasi berangka, air dan metanol

telah digunakan sebagai bendalir bekerja, dan air yang digunakan sebagai bendali bekerja menghasilkan perubahan kecil pada suhu dan kejatuhan tekanan berbanding dengan methanol sebagai bendalir bekerja. Kedua-dua bendalir bekerja; air dan methanol, ketelapan bahagian berliang dan tebal bahagian berliang memberikan kesan penting ke atas perbezaan suhu dan kejatuhan tekanan. Keputusan pengoptimuman dengan menggunakan D-optimal bagi perisian RSM menunjukkan prestasi paip haba berbentuk-L telah meningkat.

# **EXPERIMENTAL AND NUMERICAL STUDIES ON THERMAL ANALYSIS OF HEAT PIPES FOR COMPUTER COOLING APPLICATIONS**

## **ABSTRACT**

In computer industry, the growing development and demand for processing power necessitate efficient design of processors to conduct operations faster; consequently, the need for cooling techniques to dissipate the associated heat is quite obvious. Hence, it is highly desirable to explore high-performance cooling devices, especially for CPU cooling. In the present study, multi and twin U-shape vertical heat pipes, and single L-shape horizontal heat pipe, were investigated experimentally and numerically. Thermal analysis was performed under both natural and forced convection modes. The simulations were carried out in two models; the first was 3D model based on the heat transfer by conduction where the heat pipe as a whole was modeled by assuming it as a conducting medium, without taking into account the events occurring inside the heat pipe. The second was 2D model to characterize the working fluid inside the heat pipe. As an excellent tool for experimental design and optimization, design of experiment (DOE) was employed to optimize the coolant velocity and the heat input to get the best performance of the heat pipe. The results show that the air velocity and power input have important effect on the performance of finned heat pipes. The total thermal resistance decreases with increase in heat input and coolant velocity. The lowest value of the total thermal resistances for finned U-shape multi heat pipe, twin heat pipe and single L-shape heat pipe are  $0.181\text{ }^{\circ}\text{C/W}$ ,  $0.125^{\circ}\text{C/W}$  and  $0.533\text{ }^{\circ}\text{C/W}$  respectively. In

the numerical simulation, water and methanol were used as working fluids, and the use of water as working fluid resulted in small temperature difference and pressure drop compared to that with methanol as working fluid. For both working fluids; water and methanol, the wick permeability and wick thickness have major effects on temperature difference and pressure drop. The result of the optimization using D-optimal of RSM software reveals that the performance of L-shape heat pipe is improved.



# CHAPTER 1

## INTRODUCTION

### **1.1 Introduction**

Effective cooling of electronic components is important for the successful functioning and high reliability of the electronic devices. The rapid developments in microprocessors necessitate enhanced processing power to ensure faster operations; consequently, the need for cooling techniques to dissipate the associated heat is quite obvious. Moreover, the present standard metallic heat sinks are obsolete in many ways and are not sufficient to address the increased cooling needs that are sought by many of today's electronic devices. Hence, it is highly desirable to explore high-performance cooling devices, especially for CPU cooling. Heat pipe has been identified and proved as one of the viable and promising options to achieved this purpose, due to its simple structure, flexibility and in particular, high efficiency.

### **1.2 Heat Pipe**

Heat pipe is one of the most efficient heat transport devices; it makes use of phase change of the working fluid inside, in order to facilitate the heat transport. The heat pipes are best for cooling electronic devices as their thermal conductivity is several hundreds more than that of a copper rod. Heat pipe which was proposed by Gaugler in 1942 as a cooling strategy for electronic apparatus, is a promising alternative compared to the conventional cooling schemes. As shown in the Figure 1.1, the main perception of a heat pipe involves passive two-phase heat transfer device that facilitate minimum drop

in temperature by transferring large quantity of heat. By employing such devices, higher local heat removal is possible and uniform heat dissipation can be attained.

Several day-to-day gadgets such as heat exchangers, air-conditioners, refrigerators, transistors and capacitors employ heat pipes. Heat pipes are also used in desktops and laptops to decrease the operating temperature for better performance. Heat pipes are commercially presented since the mid 1960's. Electronic cooling has just embraced heat pipe as a dependable and cost-effective solution for sophisticated cooling application.

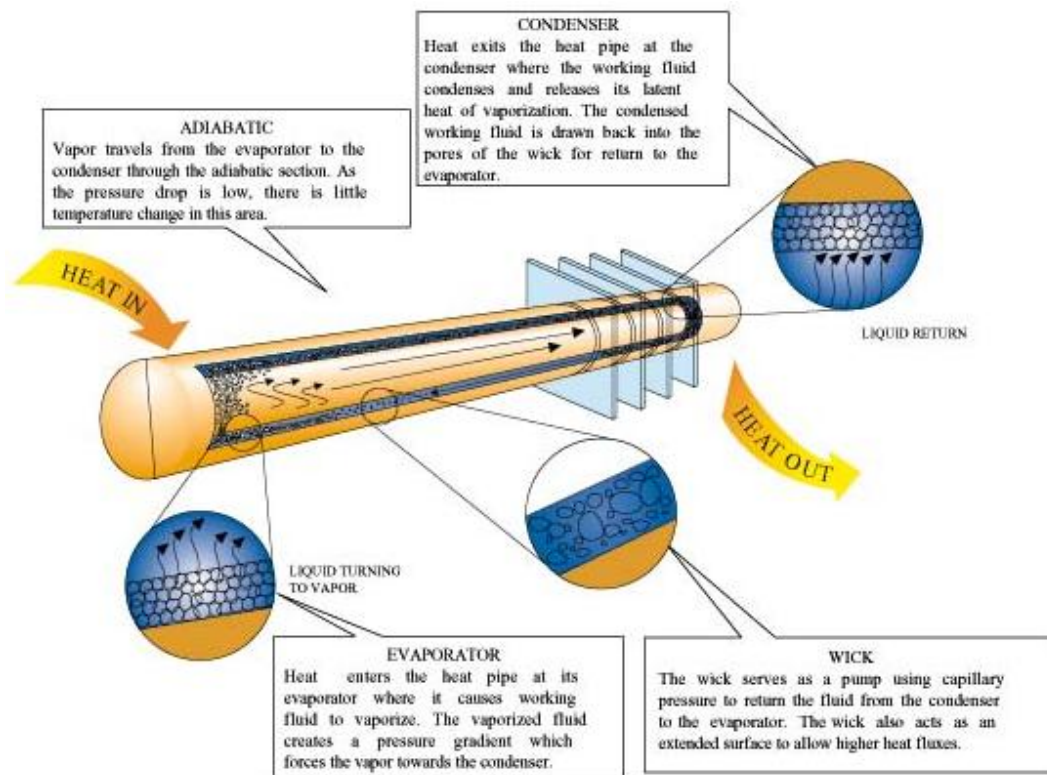


Figure 1.1: Heat pipe operation (<http://www.electronics-cooling.com>).

### **1.2.1 Historical background**

Perkins tube can be historically traced as the first evolved concept of the heat pipe, and the thermosyphon, also named as Perkins pipes, was invented by Perkins in 1897 (Peterson, 1994). The thermosyphon was the precursor of the heat pipe. It operates without wick conductor; the heat transfer is achieved through the latent heat of evaporation and the liquid return to the evaporator due to gravity. Unwicked pipes were used long before the appearance of heat pipes in the construction industry; the important milestone in their development was the use of capillary forces in vapor-liquid heat conductors.

The idea of constructor in which the heat transfer was achieved using the evaporation and condensation of a working medium was proposed by Gaugler in 1942 (Dunn and Reay, 1982). In this device, there was a porous wick container in which the liquid was returned to the evaporator through it by capillary flow. This concept was re-invented by Grover and his co-workers at Los Alamos in 1963 (Ivanovskii, 1982). In that case, the working fluid return was by the capillary force. Grover verified the efficiency of heat pipes as a high performance heat transmission device and developed several applications. This development has brought about the rebirth of a high-performance device called the heat pipe.

### **1.2.2 Construction of heat pipe**

There are three basic components of a heat pipe: container, working fluid and wick or capillary structure:

### **1.2.2.1 Container**

Container is a metal seal, which is capable of transferring heat through it to the working fluid. This metal has good heat conductivity. Many factors affect the selection of material of the container. Among them wettability, strength to weight ratio, machinability and ductility, compatibility with external environment and working fluid, thermal conductivity, including weldability and porosity are very important. The container material must possess high strength to weight ratio, it must be non-porous in order to avoid any diffusion of vapor particles, and at the same time should ensure minimum temperature difference between the wick and the heat source owing to its higher thermal conductivity.

### **1.2.2.2 Working fluid**

Selection of the working fluid depends primarily on the operating vapor temperature range. This is because the basis in the operation of the heat pipe is the process of evaporation and condensation of the working fluid. The selection of appropriate working fluid must be done carefully, taking into account the following factors:

- Must have very high surface tension
- Should demonstrate good thermal stability
- Wettability of wall materials and wick
- Should have high latent heat
- Should possess high thermal conductivity
- Should have low liquid and vapor viscosities, and
- it must be compatible with both wall materials and wick

The most important property of the working fluid is high surface tension so that the heat pipe works against gravity as it generates high force of the capillarity characteristic. Table 1 summarizes the properties of some working fluids with their useful ranges of temperature (Dunn and Reay, 1982).

Table 1.1: Heat pipe working fluids properties (Dunn and Reay, 1982)

<b>Medium</b>	<b>Melting Point (° C )</b>	<b>Boiling Point (°C)</b>	<b>Useful Range (°C)</b>
Helium	- 271	- 261	-271 to -269
Nitrogen	- 210	- 196	-203 to -160
Ammonia	- 78	- 33	-60 to 100
Acetone	- 95	57	0 to 120
Methanol	- 98	64	10 to 130
Flutec PP2	- 50	76	10 to 160
Ethanol	- 112	78	0 to 130
Water	0	100	30 to 200
Toluene	- 95	110	50 to 200
Mercury	- 39	361	250 to 650
Sodium	98	892	600 to 1200
Lithium	179	1340	1000 to 1800
Silver	960	2212	1800 to 2300

### 1.2.2.3 Wick or Capillary Structure

The wick develops the necessary capillary pressure which in turn facilitates the return of the working fluid from the condenser section to the evaporator section. The decrease in the pore size of the wick structure produces decreased wick permeability, which leads to increase the maximum capillary head generated by the wick. The thermal resistance at the evaporator section depends on the conductivity of the working fluid

through the wick. The common wick types in the electronics industry are explained as follows:

- **Metal sintered Powder wick**

As shown in the Figure 1.2 this type of the wick has a small pore size, resulting in low wick permeability, leading to the generation of high capillary forces for anti-gravity applications. The heat pipe that carries this type of wick gives small differences in temperature between evaporator and condenser section. This reduces the thermal resistance and increases the effective thermal conductivity of the heat pipe.



Figure 1.2: Metal sintered Powder wick (<http://www.frostytech.com>)

- **Grooved wick**

Grooved wick is shown in Figure 1.3; this type of wick generates a small capillary driving force, but is appropriate or sufficient for low power heat pipes which operate horizontally or with the direction of gravity.



Figure 1.3: Grooved wick (<http://www.frostytech.com>)

- **Screen Mesh wick**

Figure 1.4 shows the screen mesh wick, which is used in many of the products, and they have demonstrated useful characteristics with respect to power transport and orientation sensitivity.



Figure 1.4: Screen Mesh wick (<http://www.frostytech.com>)

### 1.2.3 Heat pipe theory and operation

In order for heat pipe to operate, the maximum capillary pressure must be greater than the sum of all pressure drops inside the heat pipe to overcome them thus the prime criterion for the operation of a heat pipe is:

$$\Delta P_c \geq \Delta P_l + \Delta P_v + \Delta P_g \quad (1.1)$$

where,  $\Delta P_c$  is the maximum capillary force inside the wick structure;  $\Delta P_l$  is pressure drop required to return the liquid from the condenser to the evaporation section;  $\Delta P_v$  is the pressure drop to move the vapor flow from the evaporation to the condenser section; and  $\Delta P_g$  is the pressure drop caused due to the difference in gravitational potential energy (may be positive, negative or zero, depend on the heat pipe orientation and a direction).

The basic steps of heat pipe operation are summarized as follows, with reference to Figure 1.1.

- 1 – The heat added at the evaporator section by conduction through the wall of heat pipe, enables the evaporation of working fluid.
- 2- The vapor moves from the evaporator section to the condenser section under the influence of vapor pressure drop resulted by evaporation of the working fluid.
- 3- The vapor condenses in the condenser section releasing its latent heat of evaporation.
- 4- The liquid returns from the condenser section to the evaporator section through the wick under the influence of capillary force and the liquid pressure drop.



#### **1.2.4 Effective thermal resistance (or thermal conductivity) of heat pipe**

Thermal resistance is the most important parameter of the heat pipe; many variables affect the value of effective thermal resistance, such as the shape of heat pipe, lengths of evaporator and condenser sections, working fluid and wick structure. The thermal resistance of the heat pipe is very small compared to the thermal resistance of solid metals due to the small difference between the evaporator and condenser temperatures, and hence the effective thermal conductivity of the heat pipe is too large and reaches up to 500 times more than solid copper rod (El-Nasr and El-Haggar, 1996).

#### **1.2.5 Advantages of heat pipe**

The heat pipe has many advantages compared with other cooling devices; few of them are listed below:

- As the heat pipes operate on a closed two-phase cycle, the effective thermal conductivity is very high which can transport large quantity of heat with very small temperature difference between evaporator and condenser sections.
- It can transfer the heat without any moving parts so that the heat pipe is calm, noise-free, maintenance-free, and is highly dependable.
- As the heat pipe size and weight are relatively small, it can be used in cooling electronic devices.
- Heat pipe is a simple device that can work in any orientation, and can transfer heat from a place where there is no opportunity and possibility to accommodate a conventional fan; for instance, in notebooks.

- Heat pipes demonstrate precise isothermal control because of which the input heat fluxes can be varied without having to make significant changes in the operating temperature (Yeh and Chu, 2002).
- The evaporator and condenser work independently, and it needs only common liquid and vapor so that the size and shape of the region of heat addition is different from the region of heat dissipation, provided that the rate of evaporation of the fluid does not exceed the rate of condensation of the vapor. Thus, the heat fluxes generated over smaller areas can be dissipated over larger areas with lower heat fluxes.

### **1.3 Heat pipe for electronic cooling**

Due to the high effective thermal conductivity of heat pipes compared to that of traditional heat sinks, heat pipes have been proposed and selected for electronic cooling. (Groll et al., 1998) reported a meticulous review of the history and developments up to the year 1998, of the application of heat pipe technology for electronic cooling. Later on, (Vasiliev, 2005) provided an outline of miniature and micro heat pipes, conventional heat pipes, spaghetti heat pipes, loop heat pipes, pulsating heat pipes and some similar applications. (Maydanik, 2005) reported an exclusive review on developments in loop heat pipes and their applications. Few recent experimental works on the use of heat pipes in electronic cooling include those of (Naphon et al., 2009), (Wang et al., 2009), (Yong et al., 2010), and (Liu and Zhu, 2011). Cooling fins equipped with heat pipes for high power and high temperature electronic circuits and devices were simulated by (Legierski and Wiecek, 2001), and the superiority of the proposed system over the

traditional devices was demonstrated. (Kim et al., 2003) developed a cooling module in the form of remote heat exchanger using heat pipe for Pentium-IV CPU as a means to ensure enhanced cooling and reduced noise level compared to the fan-assisted ordinary heat sinks. (Saengchandr and Afzulpurkar, 2009) proposed a system that combined the advantages of heat pipe and thermoelectric modules, for desktop PCs.

Recently, (Liang and Hung, 2010) introduced heat sink with finned U-shape heat pipes were compatible for a wide range of high-frequency microprocessors and evaluated their thermal performance characteristics.

The present study focuses on various configurations of finned single, twin and multi heat pipes for desktop and notebooks PC-CPU and other electronic devices, in vertical and horizontal orientations.

#### **1.4 Problem Statement**

The growing development and demand for processing power in the computer industry necessitate efficient design of processors to conduct operations faster; consequently, the need for cooling techniques to dissipate the associated heat is quite obvious. Hence, it is highly desirable to explore high-performance cooling devices, especially for CPU cooling. The conventional way to dissipate heat from desktop computers was forced convection using a fan with a heat sink directly. However, with the smaller CPU size and increased power as encountered in modern computers, the heat flux at the CPU has significantly increased. At the same time, restrictions have been imposed on the size of heat sinks and fans, and on the noise level associated with the

increased fan speed. Consequently, there has been a growing concern for improved cooling techniques that suit the modern CPU requirements. As alternatives to the traditional heat sinks, two-phase cooling devices such as heat pipe and thermosyphon, have emerged as promising heat transfer devices; the effective thermal conductivity of a heat pipe can be 10 to 200 times more than that of a solid copper rod of the same diameter (Chang et al., 2008).

In notebook computers, the processor's surface where most heat is generated is usually small, approximately  $10\text{ mm} \times 10\text{ mm}$ . For useful cooling, the heat must spread over a larger surface area away from the processor, as the space available near the processor is limited. Therefore heat must be drawn from the processor and conveyed to a place from where it can be dissipated by conventional means. This task is successfully achieved by a heat pipe as it can be accommodated in a highly constrained space in such a way that its evaporator section communicates with the heat source while the finned condenser section is exposed to the sink. Thus heat pipe is regarded as a promising way for cooling electronic equipments.

The differences in the shape of heat pipe affect its performance as the behaviors of the fluid and the wick structure inside the heat pipe play important role in the transmission of heat. However, few works on numerical characterization by taking into account the behavior of the working fluid considered only single horizontal heat pipe, and complex configurations such as multi and twin U-shape vertical heat pipes, and single L-shape horizontal heat pipe, have not been explored so far. Therefore, the present study is unique in solving this problem.

The decrease in the pore size of the wick causes low wick permeability, which increases the maximum capillary pumping head generated by the wick to overcome the total pressure drop within heat pipe; on the other hand, the permeability should be large in order to have small liquid pressure drop and therefore higher heat transport capability. Furthermore, the effective thermal conductivity in the liquid-wick region also plays important role on the heat pipe performance as the high value of this parameter gives a small temperature drop across the wick, which increases the thermal performance of the heat pipe. The effective thermal conductivity in the liquid-wick region depends on the material of the wick structure, the working fluid properties, thickness of the wick and the type of wick structure. These parameters present conflicting properties in most wick designs. Accordingly, an optimal wick design requires harmonization between these contradictory features. To resolve this issue D-Optimal approach of DOE Software is used to obtain the optimal solution to align the competing parameters.

Additionally, the increase of fan speed to cool the fins associated with the heat pipe, could lead to a sensation or noise, and such high velocities may not be required to achieve the cooling for a given heat input. This situation calls for the optimal conditions of fan speed and heat input, with the objective of maximizing the heat removal. Hence in the present study also aim to optimize the coolant velocity and heat input to get the best performance of the heat pipe.

## **1.5 Research Objectives**

The objectives of this research are:

1. To study the thermal resistance (thermal performance) of vertical finned twin and multi U-shape and horizontal L-shape heat pipes under natural and forced convections at various heat inputs.
2. To perform numerical simulation of working fluid behavior inside the heat pipe in order to predict the velocity and pressure for liquid and vapor and the wall temperature, using FEM based ANSYS software and to validate by experimental results.
3. To study numerically the effect of thickness and permeability of wick structure at different working fluids on heat pipe performance.
4. To perform the optimization using Design-Expert Software (DOE) to get the best performance of the heat pipe.

## **1.6 Thesis Outline**

This dissertation is organized in five main chapters. Chapter 1 addresses the fundamentals and the application of heat pipe for electronic cooling, the problem statement and research objectives. In Chapter 2, a comprehensive review of experimental and numerical studies on various types of heat pipes used for cooling the electronic devices and studies on the heat pipe components such as wick structure, working fluids and vapor flow are presented. Chapter 3 gives a detailed account of the materials and methods used in the current research. Deep analysis and discussion on the

results from experiments and numerical simulations are presented in Chapter 4 followed by the conclusion and suggestions for future work in Chapter 5. The dissertation ends up with references.

## CHAPTER 2

### LITERATURE REVIEW

#### 2.1 Cooling methods of electronic equipments

The air-cooling is the most important technology that contribute to the cooling of electronic devices (Ledezma and Bejan, 1996). In the past, there were three main ways to cool the electronic equipment; 1) passive air cooling that dissipates heat using the airflow generated by differences in temperature, 2) forced air cooling that dissipates heat by forcing air to flow by using fans, and 3) forced liquid cooling that dissipates heat by forcing coolants like water to pass (Suzuki and Hirano, 1998).

The conventional way to dissipate heat from desktop computers was forced convection using a fan with a heat sink directly. The advantages such as simple machining, simple structure and lower cost has made heat sinks with plate fins very useful in cooling of electronic devices (Ismail et al., 2008). However, with the smaller CPU size and increased power as encountered in modern computers, the heat flux at the CPU has significantly increased (Webb, 2005). At the same time, restrictions have been imposed on the size of heat sinks and fans, and on the noise level associated with the increased fan speed. Consequently, there has been a growing concern for improved cooling techniques that suit the modern CPU requirements. As alternatives to the conventional heat sinks, two-phase cooling devices such as heat pipe and thermosyphon, have emerged as promising heat transfer devices with effective thermal conductivity over 200 times higher than that of copper (Chang et al., 2008).



## 2.2 Thermal Design Power (TDP)

The Thermal Design Power (TDP) has attracted the topmost interest of thermal solution designers and it refers to the maximum power dissipated by a processor across a variety of applications (Mahajan et al., 2006). The purpose of TDP is to introduce thermal solutions which can inform manufacturers of how much heat their solution should dissipate. Typically, TDP is estimated as 20% - 30% lower than the CPU maximum power dissipation. Maximum power dissipation is the maximum power a CPU can dissipate under the worst conditions such as the maximum temperature, maximum core voltage, and maximum signal loading conditions. Whereas the minimum power dissipation refers to the power dissipated by the processor when it is switched into one of low-power modes. As shown in Table 2.1, the maximum TDP ranges from 35 W to 77 W for modern processors such as Intel® Core™ i5-3400 Desktop Processor Series. While the maximum TDP for modern notebook computers ranges from 17 W to 35 W as shown in Table 2.2.

Table (2.1): Maximum TDP for modern desktop computer

<http://ark.intel.com/products/series/64902>

Product Name	Max TDP	Graphics
Intel® Core™ i5-3475S Processor (6M Cache, up to 3.60 GHz)	65 W	Intel® HD Graphics 4000
Intel® Core™ i5-3470T Processor (3M Cache, up to 3.60 GHz)	35 W	Intel® HD Graphics 2500
Intel® Core™ i5-3470S Processor (6M Cache, up to 3.60 GHz)	65 W	Intel® HD Graphics 2500
Intel® Core™ i5-3470 Processor (6M Cache, up to 3.60 GHz)	77 W	Intel® HD Graphics 2500
Intel® Core™ i5-3450S Processor (6M Cache, up to 3.50 GHz)	65 W	Intel® HD Graphics 2500
Intel® Core™ i5-3450 Processor (6M Cache, up to 3.50 GHz)	77 W	Intel® HD Graphics 2500

Table 2.2: Maximum TDP for modern notebook computers  
[www.makeuseof.com/tag/thermal-design-power-technology-explained](http://www.makeuseof.com/tag/thermal-design-power-technology-explained)

Processor Number	Cache	Clock Speed	# of Cores / # of Threads	Max TDP
32 nm				
i5-2557M	3.0 MB	1.70 GHz	2 / 4	17 W
i5-2540M	3.0 MB	2.60 GHz	2 / 4	35 W
i5-2537M	3.0 MB	1.40 GHz	2 / 4	17 W
i5-2520M	3.0 MB	2.50 GHz	2 / 4	35 W

### 2.3 Experimental studies of the heat pipe

Substantial amount of experimental works have been conducted on the heat pipe to identify its thermal performance through calculations of thermal resistance of the heat pipe. Most of the experiments proved that heat pipe is the best tool for cooling the electronic devices.

(El-Nasr and El-Haggar, 1996) investigated experimentally the effects of the number of wick layers, container materials, and working fluids on the effective thermal conductivities of several heat pipes. The results indicated that, increasing the number of wick layers inside the heat pipe improved the effective thermal conductivity of the heat pipe, and increased the heat flux transferred, with low temperature drop between the evaporator section and the condenser section. In addition, the working fluid at the operating temperature range of (313-373 K) has strongly affected the heat pipe effective

thermal conductivity at steady state while the container material had faintly affected the effective thermal conductivity of the heat pipe.

(Seok-Hwan et al., 2001) studied experimentally a new woven-wire-type wick for Miniature Heat Pipes (MHP), which had a high productivity and a large capillary limit. They used MHP with diameters of 3 mm or 4 mm which could be used for notebook- CPU cooling. The design factors discussed were evaporator length and condenser length, heat pipe length, fill ratio of working fluid, number of wick strand, inclination angle of installation and thermal load. The results showed that the minimum thermal resistance was achieved when the fill ratios were 29.3% and 31% respectively, for MHPs of 3 mm and 4mm, provided with woven-wire wicks.

A novel dynamic test method in order to quantify the thermal performances of heat pipes was introduced by (Tsai et al., 2010). This method was compared with the traditional steady-state methods. As shown in the Figure 2.1a, in the steady state test, DC power supply powered the heater. The cooling jacket connected to a constant temperature circulator with a 700 W heat dissipation capacity provides the necessary cooling effect to condensation section and the heat pipe was horizontally oriented. In the Dynamic test, the evaporator section was immersed in hot water working as power supply and the heat dissipated by using fans at condenser section with the heat pipe vertically oriented as shown in Fig. 2.1b. Some of the parameters affecting the thermal performance of heat pipes, such as fill ratio, bending angle, and shape of heat pipe under both dynamic and steady state tests were investigated. Experimental results demonstrated that the operation limitations were increased when the fill ratio was increased, leading to less temperature responses of heat pipes. The effects of parameters

in both the dynamic test and the steady-state test were almost analogical. Therefore, when high efficiency is of prime importance then dynamic test would take precedence over the steady state test.

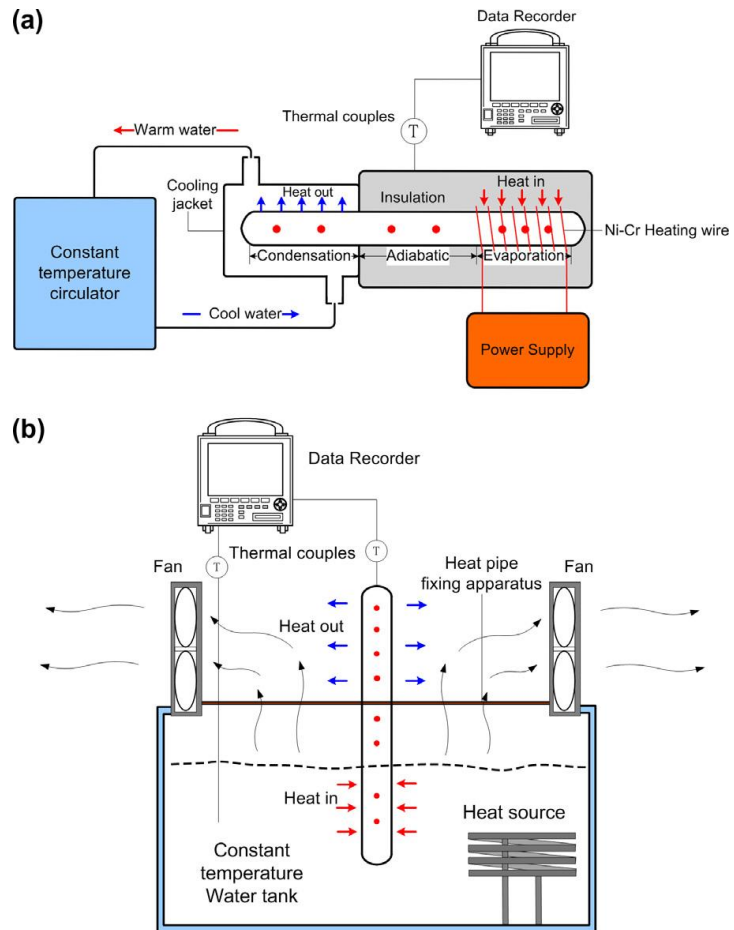


Figure 2.1: Experimental set-ups. (a) Steady-state test. (b) Dynamic test (Tsai et al., 2010).

Abundance of experiments have been performed on the heat pipes and further reviews will be carried out by studying the types of heat pipes.

## **2.4 Types of heat pipes**

### **2.4.1 Cylindrical heat pipe**

Cylindrical heat pipe with closed-ends is a common and conventional type of heat pipe. It involves circulation of working fluid and a wick to return the liquid. Basically, it consists of three sections, namely, evaporator, adiabatic and condenser.

(El-Genk and Lianmin, 1993) reported an experimental investigation of the transient response of cylindrical copper heat pipe with water as working fluid. The copper heat pipe with copper screen wick consisted of two layers of 150 meshes. The results showed that the temperature of the vapor was uniform along the heat pipe while the wall temperature drop was very small (maximum variation less than 5 K) between the evaporator section and the condenser section. When the heat input was increased or the cooling water flow rate was decreased, the steady-state value of the vapor temperature increased.

(Said and Akash, 1999) had studied experimentally the performance of cylindrical heat pipe using two types of heat pipes with and without wick, and water as the working fluid. They also studied the impact of inclined angle on the performance of heat pipe at different angles 30°, 60° and 90° with the horizontal. The results showed that the performance of the heat pipe with wick was better than the heat pipe without wick. The overall heat transfer coefficient was the best at the angle of 90 °.

(Mistry et al., 2010) carried out two-dimensional transient and steady-state numerical analysis to study the characteristics of a cylindrical copper-water wicked (80 mesh SS-304 screen) heat pipe with water as a coolant at a constant heat input. Finite

difference and Euler's explicit method (marching scheme) was utilized to solve the governing equations. As shown in Figure 2.2, a two-dimensional computational study utilizing the concept of a growing thermal layer in the wall and the wick region was carried out. The transient axial temperatures were experimentally determined and results of all the three sections of the heat pipe were then compared with that of 2D numerical solution. The time required to reach steady state was obtained. The transient and steady state predictions of temperatures from the two-dimensional model were in close agreement with the experimentally obtained temperature profiles.

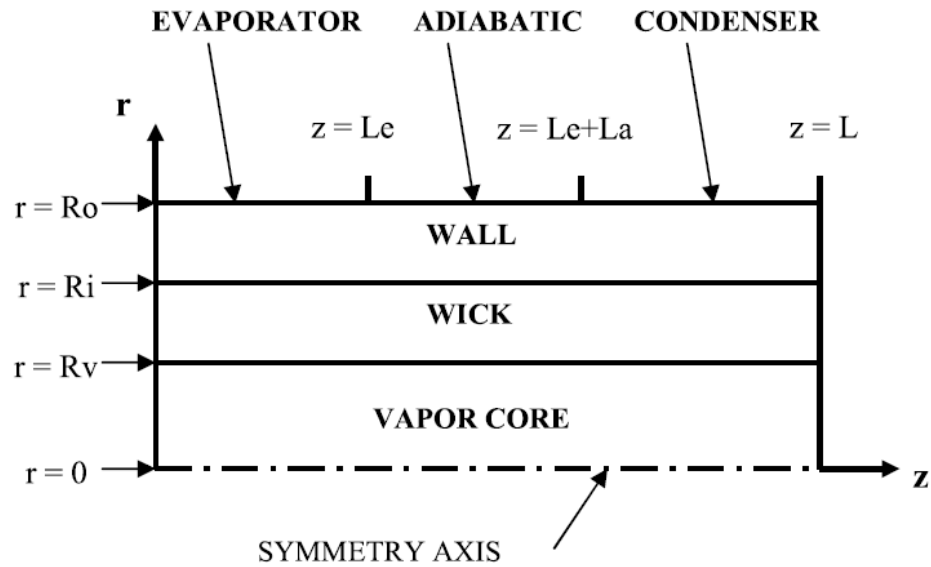


Figure 2.2: Coordinate system of the heat pipe (Mistry et al., 2010).

Further reviews of the cylindrical heat pipe will be elaborated in the numerical studies.

### 2.4.2 Flat heat pipes

(Wang and Vafai, 2000) presented an experimental investigation of the thermal performance of asymmetric flat plate heat pipe. As shown in the figure 2.3, the flat heat pipe consists of four sections which are the evaporation in the middle and three condenser sections. The heat transfer coefficient and the temperature distribution were obtained. The results indicated that the temperature was uniform along the wall surfaces of the heat pipe, and the porous wick of the evaporator section had significant effect on the thermal resistance. It was also showed that the heat transfer coefficient was  $12.4 \text{ W/m}^2 \text{ }^\circ\text{C}$  at the range of input heat flux  $425\text{-}1780 \text{ W/m}^2$ .

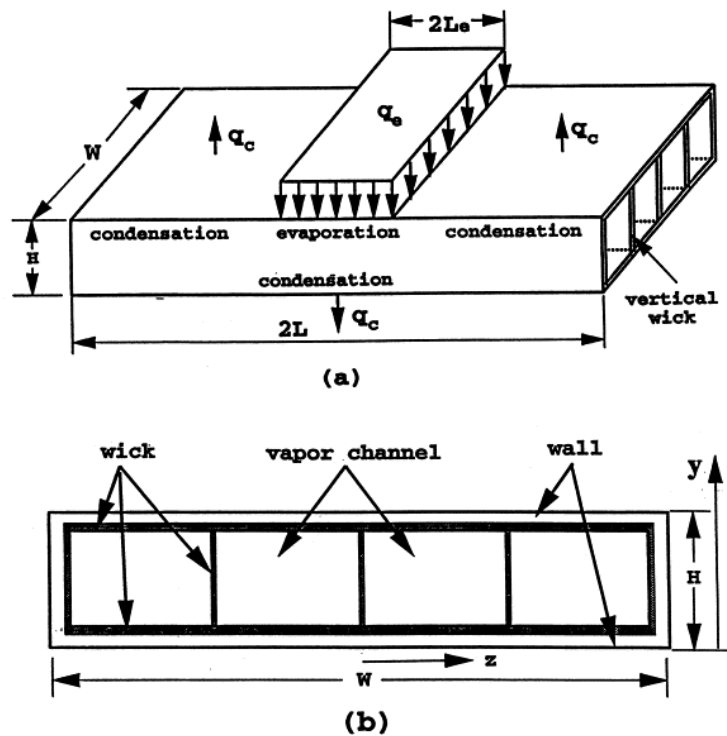


Figure 2.3: Schematic of the flat plate heat pipe: (a) geometry of the heat pipe and (b) cross-sectional view of the heat pipe (Wang and Vafai, 2000).

(Maziuk et al., 2001) modeled a flat miniature heat-pipe to determine the thermal resistance and heat transfer coefficient. The wick structure of the heat pipe was copper sintered powder. They verified the model by comparing with the experimental results. The results indicated that the wick with copper sintered powder has strong effect to enhance the performance of the flat miniature heat pipe.

Thermal performance of a flat heat pipe thermal spreader was investigated by (Carbajal et al., 2007). They carried out quasi-3D numerical analysis in order to determine the field variable distributions and the effects of parametric variations in the flat heat pipe system. The flat heat pipe which operated as a thermal spreader was able to uniformly distribute the temperature at the condenser end, in contrast to a system having a solid aluminum plate subjected to similar boundary conditions and heat input.

### **2.4.3 Micro heat pipes**

One of the characteristic features of micro-heat pipes which makes it different from the conventional heat pipes is that the sharp-angled corners replace the wick structure which provides the necessary capillary pressure for driving the liquid phase.

A substantial body of literature conceptualized micro-heat pipe as a key tool in electronics cooling since it was first proposed by (Cotter, 1984). Thus, one dimensional analytical models that analyze the liquid and vapor flow along micro-heat pipe were developed by (Babin et al., 1990), (Khrustalev and Faghri, 1994), (Longtin et al., 1994), (Peterson and Ma, 1996), (Ha and Peterson, 1998), (Ma and Peterson, 1998), (Sobhan